Neoplasma 2026; 73(5): 335–347

doi:10.4149/neo_2026_260310N61

Transcriptomic analysis of vitamin D3 (cholecalciferol)-mediated attenuation of cisplatin sensitivity in gastric cancer cells *in vitro*

Ke CHEN*, Yu PAN

Department of General Surgery, Sir Run Run Shaw Hospital, School of Medicine, Zhejiang University, Hangzhou, Zhejiang, China

**Correspondence: chenke68@zju.edu.cn*

Received March 10, 2026 / Accepted July 20, 2026

Cisplatin remains a cornerstone of chemotherapy for gastric cancer, but acquired resistance frequently limits its therapeutic efficacy. Vitamin D3/cholecalciferol (VD3) is widely used as a nutritional supplement; however, its influence on cisplatin responsiveness in gastric cancer cells remains unclear. In this study, gastric cancer cell lines were treated with cisplatin in the presence or absence of VD3, and cell viability, apoptosis, reactive oxygen species (ROS) accumulation, DNA damage-associated signaling, and transcriptomic changes were evaluated. VD3 significantly attenuated cisplatin-induced cytotoxicity in AGS, HGC-27, and MKN-45 cells. Co-treatment with VD3 reduced cisplatin-induced apoptosis, ROS accumulation, PARP cleavage, and γH2AX activation. Transcriptomic analysis showed that VD3 markedly reduced the number of cisplatin-responsive differentially expressed genes and altered gene programs associated with extracellular matrix organization, steroid metabolism, DNA damage response, and ABC transporter-related pathways. These findings suggest that VD3 exposure can attenuate cisplatin-induced cellular responses in gastric cancer cells and modulate transcriptional programs associated with cisplatin treatment. Given that the study was performed under *in vitro* conditions, further investigations are required to determine the underlying mechanisms and the potential clinical relevance of these observations.

Key words: gastric cancer; cholecalciferol; cisplatin resistance; transcriptome sequencing; apoptosis

Gastric cancer is the fifth most common cancer worldwide and the third leading cause of cancer-related death [1, 2]. Because early-stage gastric cancer often lacks specific symptoms and reliable diagnostic biomarkers, many patients are diagnosed only after the disease has progressed to an advanced stage, contributing to its high mortality rate [3]. In 2018, gastric cancer accounted for approximately 784,000 deaths globally [1]. Surgical resection, combined with chemotherapy and radiotherapy, remains the cornerstone of treatment. Cisplatin (DDP) is a first-line chemotherapeutic agent for gastric cancer, particularly in advanced disease; however, acquired resistance frequently develops and is associated with poor clinical outcomes [4].

DDP exerts its antitumor effects primarily by forming DNA cross-links that trigger DNA damage and apoptosis. However, prolonged exposure can activate DNA repair mechanisms and other adaptive responses in cancer cells, thereby reducing treatment efficacy. The mechanisms underlying DDP resistance in gastric cancer are complex and multifactorial. In addition to enhanced DNA repair, reduced intracellular drug accumulation, altered drug targets, and dysregulation of cell survival and death pathways have all been implicated in the development of resistance [5]. Several signaling pathways, including PI3K/AKT, NF-κB, MAPK, and STAT3, also contribute to the regulation of DDP responsiveness [6–9]. In gastric cancer, resistance is further influenced by marked molecular and phenotypic heterogeneity. Gastric cancer cells may acquire resistance through increased drug efflux, glutathione-dependent detoxification, impaired apoptosis, epithelial-mesenchymal transition, cancer stemness, autophagy, metabolic reprogramming, and tumor microenvironment-derived survival signals [10]. Hypoxia/HIF-1α signaling has also been closely linked to chemoresistance by promoting stemness, epithelial-mesenchymal transition, metabolic adaptation, anti-apoptotic signaling, and the expression of drug efflux transporters [11]. Together, these mechanisms contribute to heterogeneous responses to DDP and highlight the need to identify additional factors that modulate DDP sensitivity. A better understanding of these regulatory mechanisms may facilitate the development of more effective therapeutic strategies for overcoming DDP resistance in gastric cancer.

Copyright © 2026 The Authors.
This article is licensed under a Creative Commons Attribution 4.0 International License, which permits use, sharing, adaptation, distribution, and reproduction in any medium or format, as long as you give appropriate credit to the original author(s) and the source and provide a link to the Creative Commons licence. To view a copy of this license, visit https://creativecommons.org/licenses/by/4.0/

Vitamin D_3/cholecalciferol (VD_3) is a secosteroid obtained from dietary sources or synthesized endogenously in the skin. Cutaneous vitamin D_3 synthesis is not a direct conversion of cholesterol into vitamin D_3. Rather, 7-dehydrocholesterol, an intermediate of the postsqualene cholesterol biosynthetic pathway, serves as the immediate precursor. Upon exposure to ultraviolet B radiation, 7-dehydrocholesterol is photochemically converted into pre-vitamin D_3, which subsequently undergoes temperature-dependent thermal isomerization to form vitamin D_3 [12]. This photochemical process also generates other cholesterol-derived secosteroidal photoproducts, including lumisterol and tachysterol, indicating that cutaneous vitamin D biology extends beyond vitamin D_3 formation alone [12]. After synthesis in the skin or dietary intake, vitamin D_3 is metabolized to 25-hydroxyvitamin D_3 and subsequently to 1,25-dihydroxyvitamin D_3, the hormonally active vitamin D metabolite. Although the kidney is the principal endocrine source of circulating 1,25-dihydroxyvitamin D_3, vitamin D activation is not confined to renal tissue. CYP27B1 is expressed in a variety of extra-renal tissues, enabling local production of active vitamin D metabolites and supporting intracrine, autocrine, and paracrine vitamin D signaling [13]. This local vitamin D metabolic and signaling axis is particularly relevant to cancer biology because both normal and malignant tissues may express CYP27B1, CYP24A1, and the vitamin D receptor (VDR), thereby influencing tissue-specific responses to vitamin D [14]. In addition to the classical CYP2R1/CYP27B1/CYP24A1 pathway, vitamin D_3 can undergo CYP11A1-initiated hydroxylation to generate non-classical vitamin D_3 hydroxyderivatives. Lumisterol can likewise be converted into biologically active metabolites [15]. These CYP11A1-derived vitamin D and lumisterol metabolites have been associated with the regulation of oxidative stress, DNA damage responses, inflammation, and cellular proliferation [15]. In cancer models, both classical and CYP11A1-derived vitamin D_3 hydroxyderivatives have demonstrated antitumor activity, partly through inhibition of GLI1 and β-catenin signaling pathways [16]. Furthermore, vitamin D signaling may interact with circadian regulatory networks through nuclear receptors such as RORs, REV-ERBs, and AhR, highlighting the complexity of vitamin D biology beyond its traditional endocrine functions [17].

Over the past several decades, the diverse physiological and pathological functions of vitamin D_3 and its metabolites have become increasingly recognized. Vitamin D signaling has been implicated in a wide range of conditions, including metabolic syndrome, viral infection, cardiovascular disease, and cancer [18–22]. Accumulating preclinical and clinical evidence suggests that vitamin D supplementation may reduce the risk of several malignancies and influence cancer incidence, progression, and mortality [23–26]. For example, epidemiological studies have reported that higher dietary intake of vitamin D_3 and calcium is associated with a reduced risk of certain cancers [27–29]. In addition, long-term administration of selected vitamin D analogs following conventional chemotherapy has been reported to decrease colorectal cancer recurrence [30]. Antitumor effects of vitamin D_3 have also been observed in colorectal, breast, pancreatic, and head and neck cancers [31–35]. Despite these findings, the role of vitamin D_3 in modulating responses to anticancer chemotherapy, particularly DDP-based treatment, remains incompletely understood.

Therefore, the present study investigated whether vitamin D_3/cholecalciferol exposure modulates DDP sensitivity in gastric cancer cells and explored the associated cellular and transcriptomic alterations. By examining the effects of vitamin D_3 on DDP-induced cytotoxicity, apoptosis, oxidative stress, DNA damage-associated signaling, and gene expression profiles, we sought to provide new insights into factors that may influence DDP responsiveness in gastric cancer. The findings may contribute to a better understanding of the biological interactions between vitamin D_3 and DDP and provide a basis for future studies evaluating their combined use in cancer therapy.

Materials and methods

Reagents and treatment. Vitamin D_3/cholecalciferol (VD_3; #S4063) and DDP (#S1166) were purchased from Selleck Chemicals (Houston, TX, USA). VD_3 was dissolved in dimethyl sulfoxide (DMSO) to prepare a stock solution and stored at –20 °C, protected from light. Cells treated with an equivalent concentration of DMSO served as the vehicle control.

Cell culture. The human gastric cancer cell lines AGS (*Homo sapiens*, female, stomach; RRID: CVCL_0139), HGC-27 (*Homo sapiens*, female, stomach; RRID: CVCL_1279), and MKN-45 (*Homo sapiens*, male, stomach; RRID: CVCL_0434) were obtained from Procell Life Science & Technology Co., Ltd. (Wuhan, China). All cell lines were authenticated by short tandem repeat (STR) profiling and confirmed to be free of mycoplasma contamination. AGS cells were cultured in F-12K medium, whereas HGC-27 and MKN-45 cells were maintained in Roswell Park Memorial Institute (RPMI)-1640 medium supplemented with 10% fetal bovine serum (FBS; Thermo Fisher Scientific, Waltham, MA, USA). All cells were incubated at 37 °C in a humidified atmosphere containing 5% CO_2.

Cytotoxicity assay. Gastric cancer cells in the logarithmic growth phase were seeded into 96-well plates at a density of 1×10^4 cells/well and allowed to attach for 24 h at 37 °C in a humidified 5% CO_2 incubator. The culture medium was then replaced with fresh medium containing the indicated concentrations of the test compounds. Each treatment was performed in triplicate wells. After 24 h of treatment, the medium was removed, and Cell Counting Kit-8 (CCK-8) reagent was added according to the manufacturer's instructions. The plates were incubated for an additional 1 h, and the optical density (OD) at 450 nm was measured using a

Synergy H1/Synergy 2 microplate reader (BioTek Instruments, Winooski, VT, USA). Cell viability was calculated relative to the corresponding vehicle control and used to evaluate treatment-induced cytotoxicity.

Quantitative real-time PCR (qRT-PCR). Total RNA was extracted from HGC-27 cells using TRIzol reagent according to the manufacturer's instructions. RNA concentration and purity were determined spectrophotometrically. Complementary DNA (cDNA) was synthesized using a reverse transcription kit. qRT-PCR was performed using SYBR Green PCR Master Mix on a real-time PCR detection system. Relative mRNA expression levels were calculated using the 2−ΔΔCt method, with GAPDH serving as the internal control. To validate the RNA-seq results, the expression levels of CYP24A1, HMGCR, GDF15, CDKN1A, and SPIDR were analyzed by qRT-PCR. The primer sequences used in this study are listed in Supplementary Table S1.

Flow cytometry. Cells were collected and washed twice with pre-cooled phosphate-buffered saline (PBS) to remove residual drug. After centrifugation at 1,500 × g for 5 min, the supernatant was discarded, and the cell pellet was resuspended in 195 μl of Annexin V-FITC binding buffer from the Annexin V-FITC/PI Apoptosis Detection Kit (Beyotime Biotechnology, Shanghai, China). Subsequently, 5 μl of Annexin V-FITC and 10 μl of propidium iodide (PI) staining solution were added. The samples were gently mixed and incubated for 15 min at room temperature in the dark. Apoptosis was then analyzed using a CyFlow flow cytometer (Sysmex Partec GmbH, Görlitz, Germany).

Western blotting. Cells were harvested and washed two to three times with 1× PBS, followed by centrifugation at 1,000×g for 5 min. After removal of the supernatant, the cell pellets were lysed in an appropriate volume of lysis buffer and incubated on ice for 10–15 min. The lysates were then centrifuged at 13,000×g for 10 min at 4 °C, and the supernatants containing total cellular proteins were collected for analysis. Protein concentrations were determined using a bicinchoninic acid (BCA) protein assay kit according to the manufacturer's instructions. Equal amounts of protein were separated by sodium dodecyl sulfate-polyacrylamide gel electrophoresis (SDS-PAGE) and transferred onto polyvinylidene fluoride (PVDF) membranes (FFP36; Beyotime Biotechnology, Shanghai, China). The membranes were blocked with 5% non-fat milk in TBST (Tris-buffered saline containing Tween 20) for 1 h at room temperature and then incubated overnight at 4 °C with the appropriate primary antibodies, including anti-cleaved PARP antibody (Cell Signaling Technology, Danvers, MA, USA), anti-H2AX antibody (Cell Signaling Technology), and anti-α-tubulin antibody (Beyotime Biotechnology). After three washes with TBST (10 min each), the membranes were incubated with the corresponding secondary antibodies for 2 h at room temperature. Protein bands were visualized using an enhanced chemiluminescence (ECL) detection reagent (Fude Biological Technology Co., Ltd., Hangzhou, China) and imaged with a ChemiDoc™ XRS+ imaging system (Bio-Rad Laboratories, Hercules, CA, USA).

Reactive oxygen species (ROS) assay. Sterile coverslips were prepared by soaking in 75% ethanol for 24 h and were subsequently washed three times with sterile PBS before being placed into 6-well plates. Gastric cancer cells in the logarithmic growth phase were seeded onto the coverslips at a density of 5×10^5 cells/well and incubated for 24 h at 37 °C in a humidified atmosphere containing 5% CO_2. The culture medium was then replaced with fresh medium containing the indicated concentrations of the test compounds, and the cells were incubated for an additional 24 h. Intracellular ROS levels were assessed using the fluorescent probe 2',7'-dichlorodihydrofluorescein diacetate (DCFH-DA). The DCFH-DA working solution was prepared by diluting the stock solution 1:1,000 in serum-free medium to a final concentration of 10 μM. After treatment, the culture medium was removed, and the DCFH-DA solution was added to each well. Cells were incubated for 20 min at 37 °C in a 5% CO_2 incubator and then washed three to five times with serum-free medium to remove excess probe. Intracellular ROS generation was visualized using a fluorescence microscope with excitation and emission wavelengths of 488 and 525 nm, respectively. Fluorescence intensity was used as an indicator of intracellular ROS levels.

Transcriptome sequencing data analysis. Total RNA samples were submitted to Jingguang Gene Technology Co., Ltd. (China) for Illumina high-throughput sequencing. Gene expression levels were quantified using the transcripts per million (TPM) method. Differential expression analysis was performed in R using the limma package after data normalization. Genes with $p<0.05$ and $|logFC|>1$ were considered differentially expressed genes (DEGs) and were selected for subsequent analyses. Functional enrichment analyses of DEGs were conducted using the clusterProfiler package to identify significantly enriched Gene Ontology (GO) terms and Kyoto Encyclopedia of Genes and Genomes (KEGG) pathways. The results were visualized using the ggplot2, pheatmap, and GOplot packages. Gene Set Enrichment Analysis (GSEA) was performed using GSEA software version 4.1.0 to evaluate the enrichment of predefined gene sets.

Protein-protein interaction (PPI) networks were constructed using the STRING database (https://string-db.org/). The interaction data were subsequently imported into Cytoscape (https://www.cytoscape.org/) for network visualization and analysis, with upregulated and downregulated genes displayed in different colors. Subnetwork analysis was performed using the MCODE plugin with the following parameters: degree cutoff ≥2, node score cutoff ≥0.2, k-core ≥2, and maximum depth = 100. Subnetworks with MCODE scores >6 were selected for further investigation.

Genes identified within the selected subnetworks were subjected to GO and KEGG annotation analyses using the ClueGO plugin to characterize their associated biological functions and signaling pathways. Finally, hub genes within

the PPI network were identified using the cytoHubba plugin based on topological network algorithms, enabling the prediction of key regulatory genes potentially involved in the observed transcriptomic changes.

Data analysis. Statistical analyses were performed using IBM SPSS Statistics (IBM Corp., Armonk, NY, USA) and GraphPad Prism (GraphPad Software, San Diego, CA, USA). Data are presented as the mean ± standard deviation (SD) from at least three independent experiments unless otherwise specified. Differences among multiple groups were evaluated using one-way analysis of variance (ANOVA). A two-sided p-value <0.05 was considered statistically significant.

Results

VD_3 decreased the sensitivity of gastric cancer cells to DDP and inhibited DDP-induced apoptosis. Before evaluating the effect of VD_3 on DDP response, we first examined the effects of different VD_3 concentrations on gastric cancer cell viability. Based on these preliminary results, VD_3 concentrations that did not show obvious cytotoxicity, namely 40 and 60 μM, were selected for combination treatment with DDP (Supplementary Figure S1). We then used the CCK-8 assay to assess the cytotoxic effects of DDP in AGS, HGC-27, and MKN-45 cells. As shown in Figure 1A, increasing DDP concentrations progressively reduced cell viability in the absence of VD_3. However, VD_3 co-treatment significantly increased cell viability compared with DDP treatment alone. Moreover, the protective effect became more evident with increasing VD_3 concentrations. These results indicate that DDP sensitivity differs among gastric cancer cell lines and that VD_3 reduces DDP sensitivity in these cells.

We next evaluated apoptosis after 24 h of treatment by flow cytometry. DDP significantly induced apoptosis in gastric cancer cells, whereas VD_3 alone had no obvious effect on the apoptotic rate. Compared with DDP treatment alone, co-treatment with VD_3 significantly reduced apoptosis (Figure 1B). Because apoptotic cells typically show chromatin condensation and nuclear fragmentation, Hoechst staining was also performed to assess nuclear morphological changes. As shown in Supplementary Figure S2, approximately one-third of AGS cells treated with DDP alone exhibited condensed or fragmented nuclei, whereas these apoptotic features were markedly reduced after VD_3 co-treatment. These findings further support that VD_3 attenuates DDP-induced apoptosis in gastric cancer cells.

VD_3 inhibits DDP-induced apoptosis by reducing PARP1 cleavage and γH2AX accumulation. To further

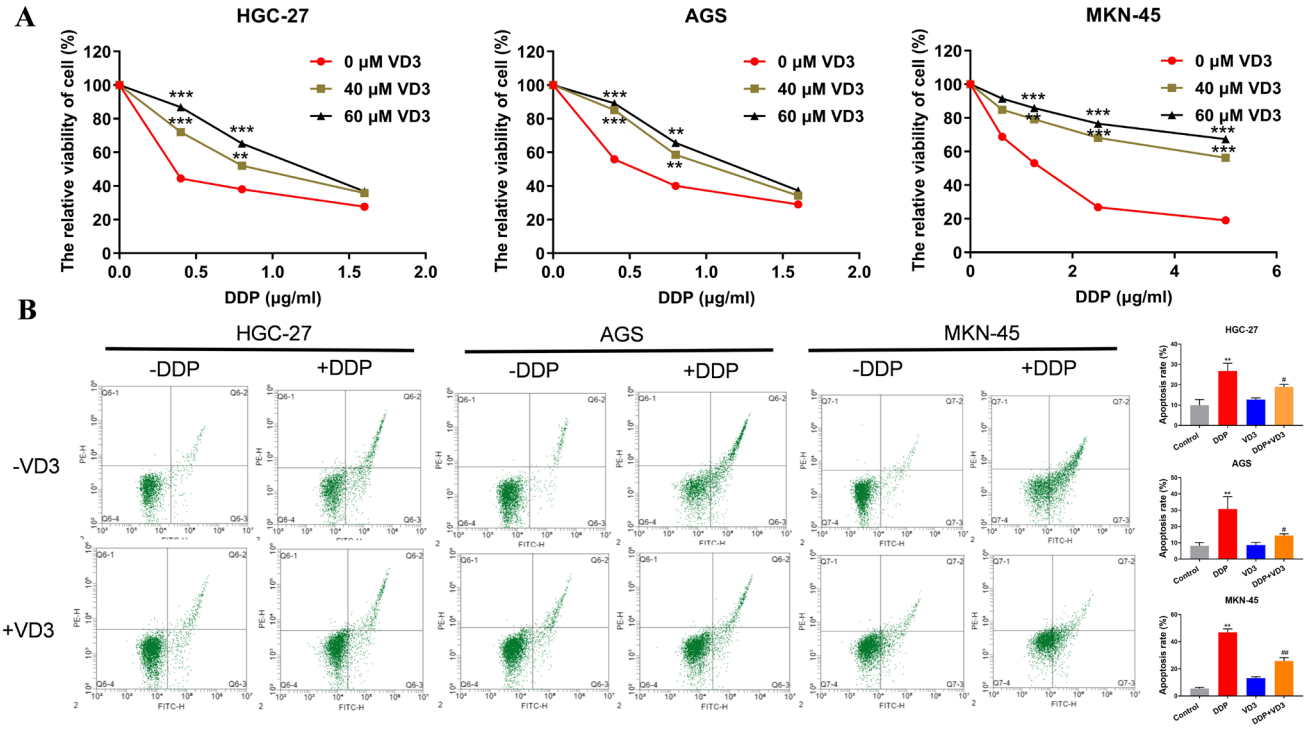

Figure 1. VD_3 attenuates DDP-induced cytotoxicity and apoptosis in gastric cancer cells. A) HGC-27, AGS, and MKN-45 cells were treated with the indicated concentrations of DDP in the presence or absence of VD_3 for 24 h, and cell viability was assessed using the CCK-8 assay. Cell viability was normalized to the corresponding vehicle control group. B) Apoptosis in HGC-27, AGS, and MKN-45 cells following treatment with vehicle control, VD_3, DDP, or DDP plus VD_3 for 24 h was analyzed by Annexin V-FITC/PI flow cytometry. Quantitative data are presented as the mean ± SD of three independent experiments. Statistical significance was determined by one-way ANOVA. **p<0.01 vs. the control group; #p<0.05 and ##p<0.01 vs. the DDP-treated group

investigate the role of VD_3 in modulating DDP-induced apoptosis, we examined PARP1 cleavage, a well-established marker of apoptotic cell death, by western blotting. As shown in Figure 2, cleaved PARP1 was undetectable in both the control and VD_3-treated groups. In contrast, DDP treatment markedly increased PARP1 cleavage in all three gastric cancer cell lines. Co-treatment with VD_3 substantially reduced the abundance of cleaved PARP1, particularly in HGC-27 and AGS cells. These findings are consistent with the flow cytometric and Hoechst staining results, further supporting the inhibitory effect of VD_3 on DDP-induced apoptosis.

Because DDP exerts its cytotoxic effects primarily through DNA damage, we next assessed γH2AX, a widely used marker of DNA damage response activation. DDP treatment markedly increased γH2AX levels in gastric cancer cells, whereas co-treatment with VD_3 attenuated DDP-induced γH2AX accumulation (Figure 2). These results indicate that VD_3 reduces the activation of DNA damage-associated signaling induced by DDP. However, it should be noted that reduced γH2AX accumulation alone does not directly demonstrate enhanced DNA repair capacity.

VD_3 reduces DDP-induced oxidative stress. Previous studies have shown that DDP can promote intracellular ROS accumulation, leading to mitochondrial dysfunction, DNA damage, and apoptosis. Given the reported antioxidant properties of VD_3, we investigated whether VD_3 modulates the oxidative stress response induced by DDP. As shown in Figure 3, DDP treatment for 24 h significantly increased intracellular ROS levels in gastric cancer cells. In contrast, co-treatment with VD_3 markedly reduced DDP-induced ROS accumulation. These findings suggest that VD_3 attenuates oxidative stress induced by DDP, which may contribute to the reduced apoptosis and γH2AX activation observed in gastric cancer cells.

The combination of VD_3 reduced the number of DDP-induced DEGs. To explore the mechanisms by which VD_3 modulates DDP sensitivity, transcriptomic analyses were performed in HGC-27 cells treated with vehicle control, DDP, VD_3, or DDP plus VD_3. Compared with the control group, DDP treatment resulted in 499 significantly upregulated genes and 514 significantly downregulated genes (Figure 4A). In contrast, VD_3 treatment alone induced relatively limited transcriptional changes, with 14 genes significantly upregulated, and 36 genes significantly downregulated (Figure 4B). Cells treated with DDP plus VD_3 exhibited 274 upregulated and 198 downregulated genes relative to the control group (Figure 4C). Furthermore, comparison of the DDP plus VD_3 group with the DDP-alone group identified 35 significantly upregulated genes and 24 significantly downregulated genes (Figure 4D).

To further evaluate the impact of VD_3 on DDP-induced transcriptional responses, overlap analysis was performed between the differentially expressed genes identified in the DDP group and those identified in the DDP plus VD_3 group. Among the 1,013 genes differentially expressed following DDP treatment, 629 were no longer significantly altered after co-treatment with VD_3, whereas 88 additional genes became differentially expressed in the presence of VD_3 (Figure 4E). These findings suggest that VD_3 substantially modifies the

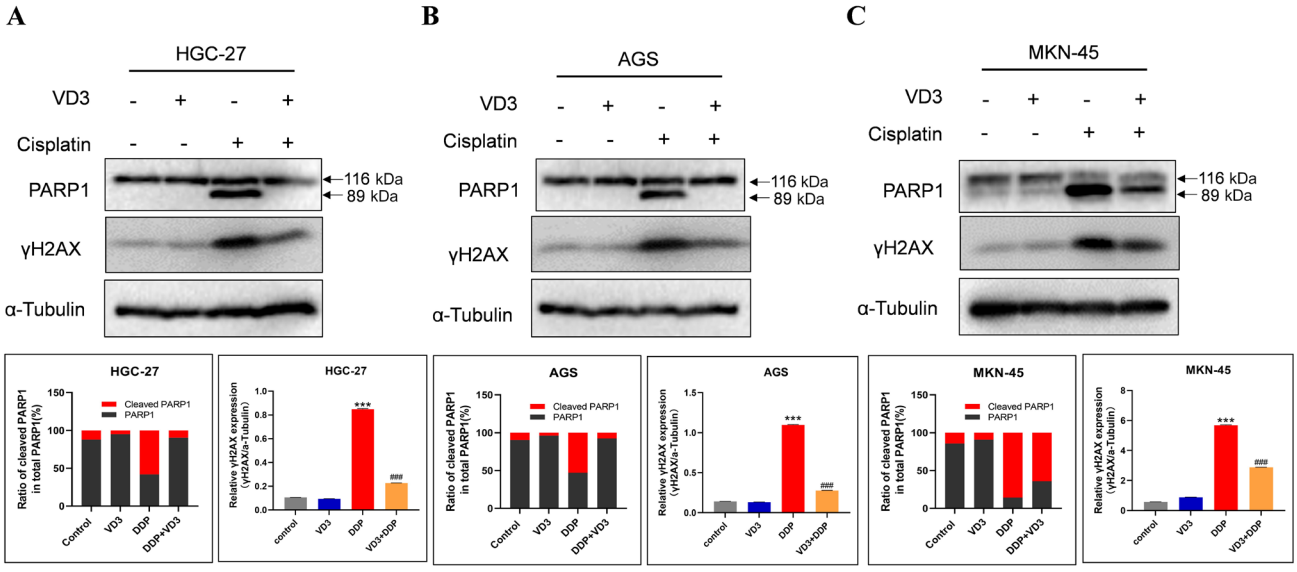

Figure 2. VD_3 reduces DDP-induced PARP1 cleavage and γH2AX accumulation. A–C) Western blot analysis of PARP1, cleaved PARP1, and γH2AX in HGC-27 (A), AGS (B), and MKN-45 (C) cells following treatment with vehicle control, VD_3, DDP, or DDP plus VD_3 for 24 h. α-Tubulin was used as the loading control. Representative immunoblots and corresponding quantitative analyses are shown. Data are presented as the mean ± SD of three independent experiments. Statistical significance was determined by one-way ANOVA. ***p<0.001 vs. the control group; ###p<0.001 vs. the DDP-treated group.

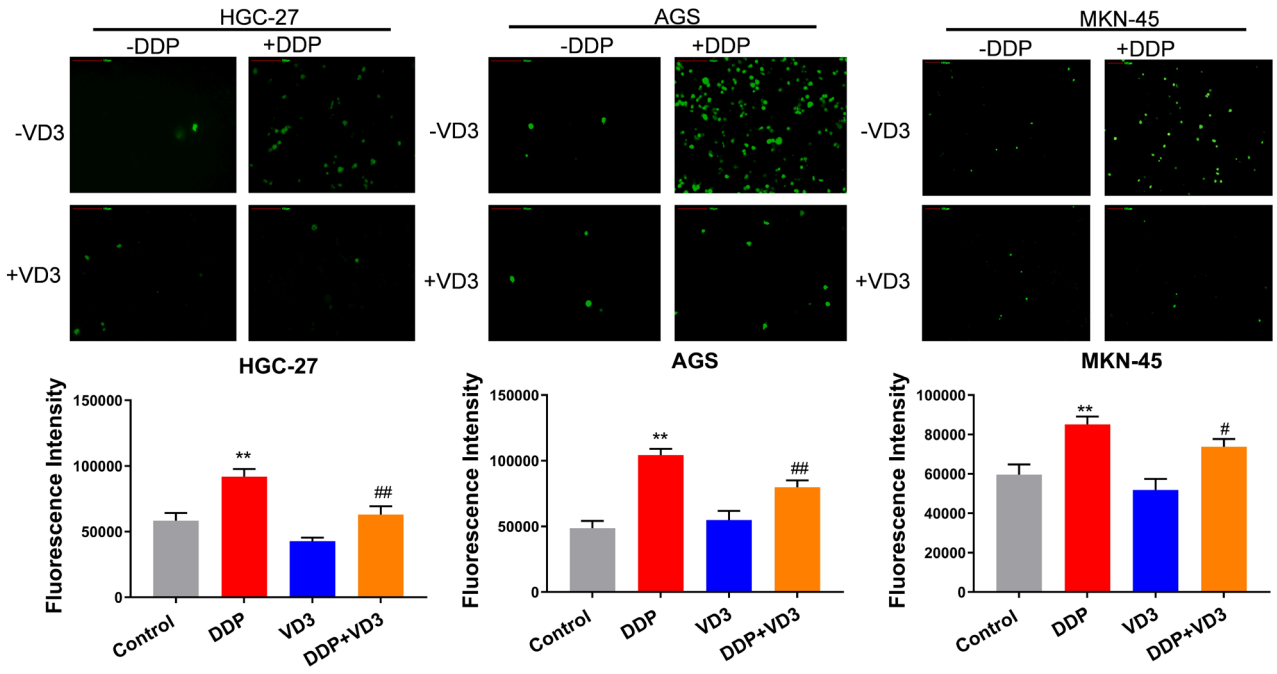

Figure 3. VD_3 attenuates DDP-induced oxidative stress in gastric cancer cells. A–C) Intracellular ROS levels in HGC-27 (A), AGS (B), and MKN-45 (C) cells following treatment with vehicle control, VD_3, DDP, or DDP plus VD_3 for 24 h were assessed using the DCFH-DA fluorescent probe. Representative fluorescence images and corresponding quantitative analyses are shown. Fluorescence intensity was normalized to the vehicle control group. Data are presented as the mean ± SD of three independent experiments. Statistical significance was determined by one-way ANOVA. **p<0.01 vs. the control group; #p<0.05 and ##p<0.01 vs. the DDP-treated group

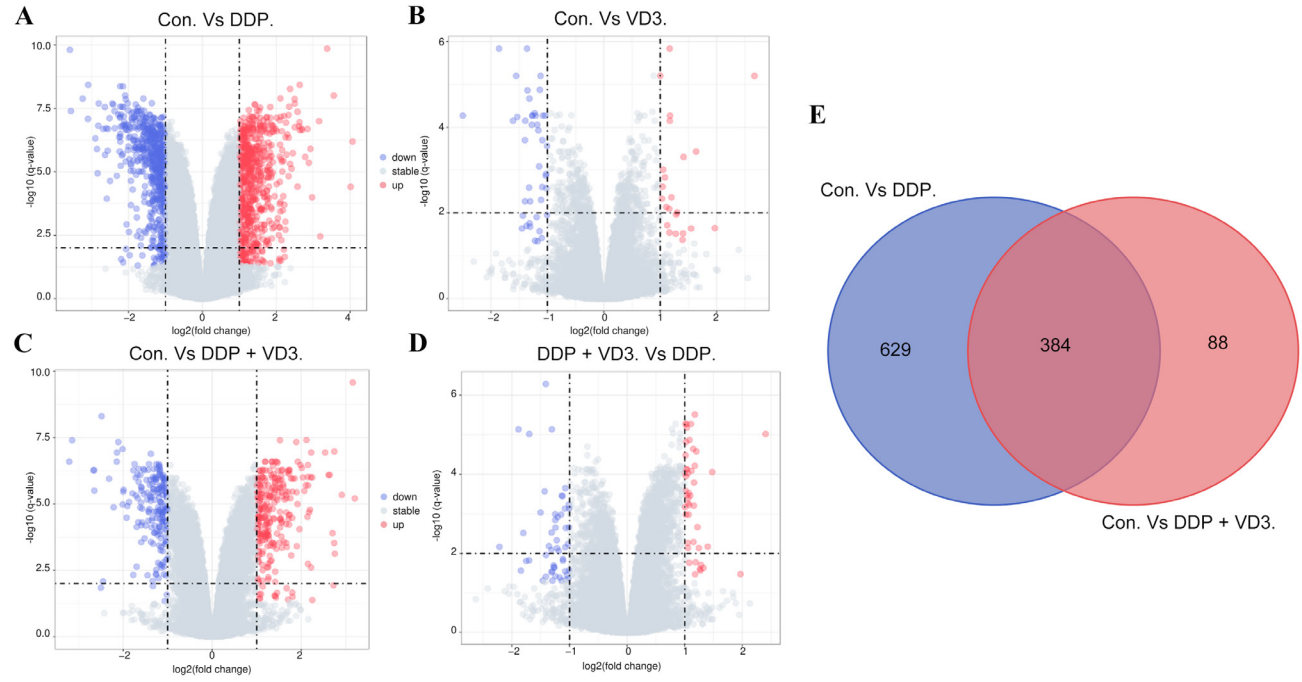

Figure 4. Transcriptomic changes among the control, DDP, VD_3, and DDP plus VD_3 groups in HGC-27 cells. RNA-seq was performed in HGC-27 cells treated with vehicle control, VD_3, DDP, or DDP plus VD_3 for 24 h. DEGs were identified using the criteria of $|\log_2 FC|>1$ and p<0.05. A–D) Volcano plots showing DEGs in the Control vs. DDP (A), Control vs. VD_3 (B), Control vs. DDP plus VD_3 (C), and DDP vs. DDP plus VD_3 (D) comparisons. Red dots represent upregulated genes, blue dots represent downregulated genes, and gray dots represent genes that were not differentially expressed. E) Venn diagram showing the overlap of DEGs among the indicated comparison groups.

transcriptional response to DDP and reduces the overall number of DDP-responsive DEGs.

VD_3 modulates DDP-responsive transcriptional programs associated with lipid metabolism. To gain further insight into the biological significance of the transcriptomic changes, we examined the 30 most DEGs across the treatment groups. As shown in Supplementary Figure S3A, DDP treatment markedly altered the expression of genes involved in cell growth, cell-cycle regulation, and DNA damage responses, including growth differentiation factor 15 (*GDF15*), cyclin-dependent kinase inhibitor 1A (*CDKN1A*), and scaffold protein involved in DNA repair (*SPIDR*). In contrast, VD_3 treatment primarily affected genes associated with lipid metabolism and vitamin D catabolism, such as 3-hydroxy-3-methylglutaryl-CoA reductase (*HMGCR*) and cytochrome P450 family 24 subfamily A member 1 (*CYP24A1*) (Supplementary Figure S3B). Following co-treatment with DDP and VD_3, *GDF15* and *CDKN1A* remained significantly altered relative to the control group, whereas SPIDR was no longer differentially expressed. In addition, genes such as *ASNS* and *CTSL* showed notable expression changes in the co-treatment group (Supplementary Figure S3C), suggesting that these genes may be involved in the cellular response to combined DDP and VD_3 treatment. Comparison of the DDP plus VD_3 group with the DDP-alone group further revealed differential expression of genes related to lipid metabolism and vitamin D catabolism, including *OLR1* and *CYP24A1* (Supplementary Figure S3D).

To validate the RNA-seq findings, selected genes were analyzed by qRT-PCR in HGC-27 cells treated with vehicle control, VD_3, DDP, or DDP plus VD_3. The validated genes included *CYP24A1*, *HMGCR*, *GDF15*, *CDKN1A*, and *SPIDR*, which are associated with vitamin D metabolism, steroid metabolism, DDP-induced stress responses, and DNA damage-associated signaling. The qRT-PCR results showed expression patterns that were generally consistent with those obtained from RNA-seq analysis, supporting the reliability of the transcriptomic data (Supplementary Figure S4).

GO-BP and KEGG enrichment analyses of differentially expressed genes. To further investigate the biological processes associated with the modulation of DDP responses by VD_3, GO biological process (GO-BP) enrichment analyses were performed on the identified differentially expressed genes. As shown in Figure 5A, DDP treatment significantly suppressed genes involved in extracellular matrix (ECM) organization while enriching genes associated with the negative regulation of protein phosphorylation. Comparison of the VD_3-treated and control groups revealed significant

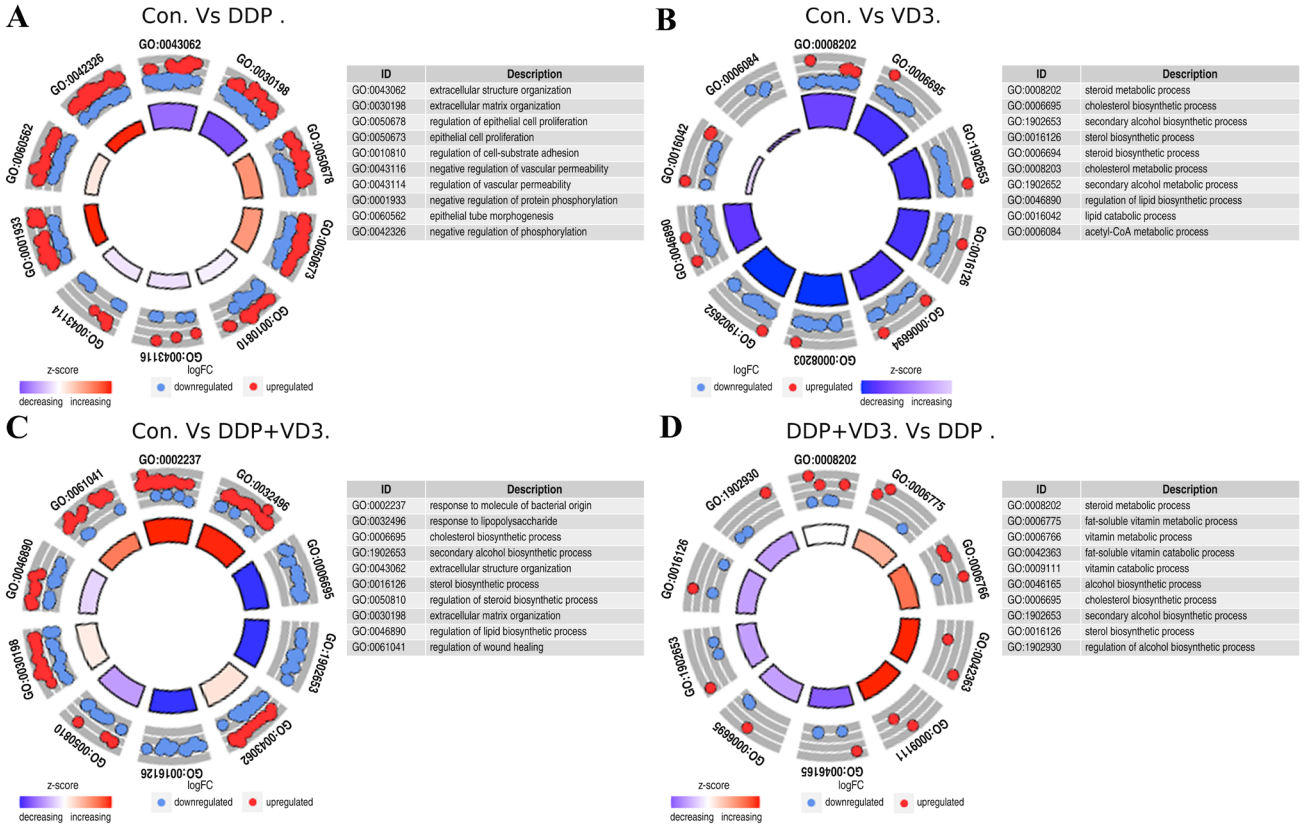

Figure 5. GO enrichment analysis of DEGs. GO biological process enrichment analysis was performed using DEGs from the indicated comparison groups: Control vs. DDP (A), Control vs. VD_3 (B), Control vs. DDP plus VD_3 (C), and DDP vs. DDP plus VD_3 (D).

enrichment of processes related to steroid metabolism, lipid catabolism, and acetyl-CoA metabolism following VD_3 treatment (Figure 5B). In cells treated with DDP plus VD_3, the downregulation of ECM-associated genes induced by DDP was partially attenuated, resulting in a modest increase in the expression of ECM-related genes compared with DDP treatment alone (Figure 5C). Furthermore, comparison of the DDP plus VD_3 group with the DDP-alone group showed enrichment of vitamin metabolic processes and suppression of steroid biosynthetic processes in the co-treatment group (Figure 5D).

To further characterize the affected signaling pathways, KEGG enrichment analyses were conducted for the differentially expressed genes identified in each comparison. As shown in Figure 6A, DDP treatment significantly affected several pathways, including the NF-κB signaling pathway, ECM-receptor interaction, and TNF signaling pathway. In contrast, VD_3 treatment primarily influenced the steroid biosynthesis pathway (Figure 6B). In the DDP plus VD_3 group, steroid biosynthesis remained one of the most prominently altered pathways, whereas ECM-receptor interaction was no longer significantly enriched (Figure 6C). When the DDP plus VD_3 group was directly compared with the DDP-alone group, relatively few pathway-level differences were observed, with steroid biosynthesis representing the principal altered pathway (Figure 6D).

GSEA analysis of signaling pathway alterations associated with VD_3 treatment. Because signaling pathway activity can be influenced by coordinated changes in multiple genes, analyses based solely on DEGs may not fully capture pathway-level alterations. Therefore, GSEA was performed using the complete transcriptomic dataset to provide a more comprehensive assessment of pathway enrichment. As relatively few DEGs were identified between the DDP plus VD_3 group and the DDP-alone group, KEGG enrichment analysis detected only a limited number of significantly enriched pathways. In contrast, GSEA revealed broader transcriptomic changes associated with VD_3 treatment. Compared with DDP treatment alone, co-treatment with VD_3 was associated with enrichment of gene sets related to ABC transporters and ECM-receptor interaction, whereas gene sets involved in steroid biosynthesis were negatively enriched (Figures 7A–7C). These findings suggest that VD_3 modulates transcriptional programs associated with trans-

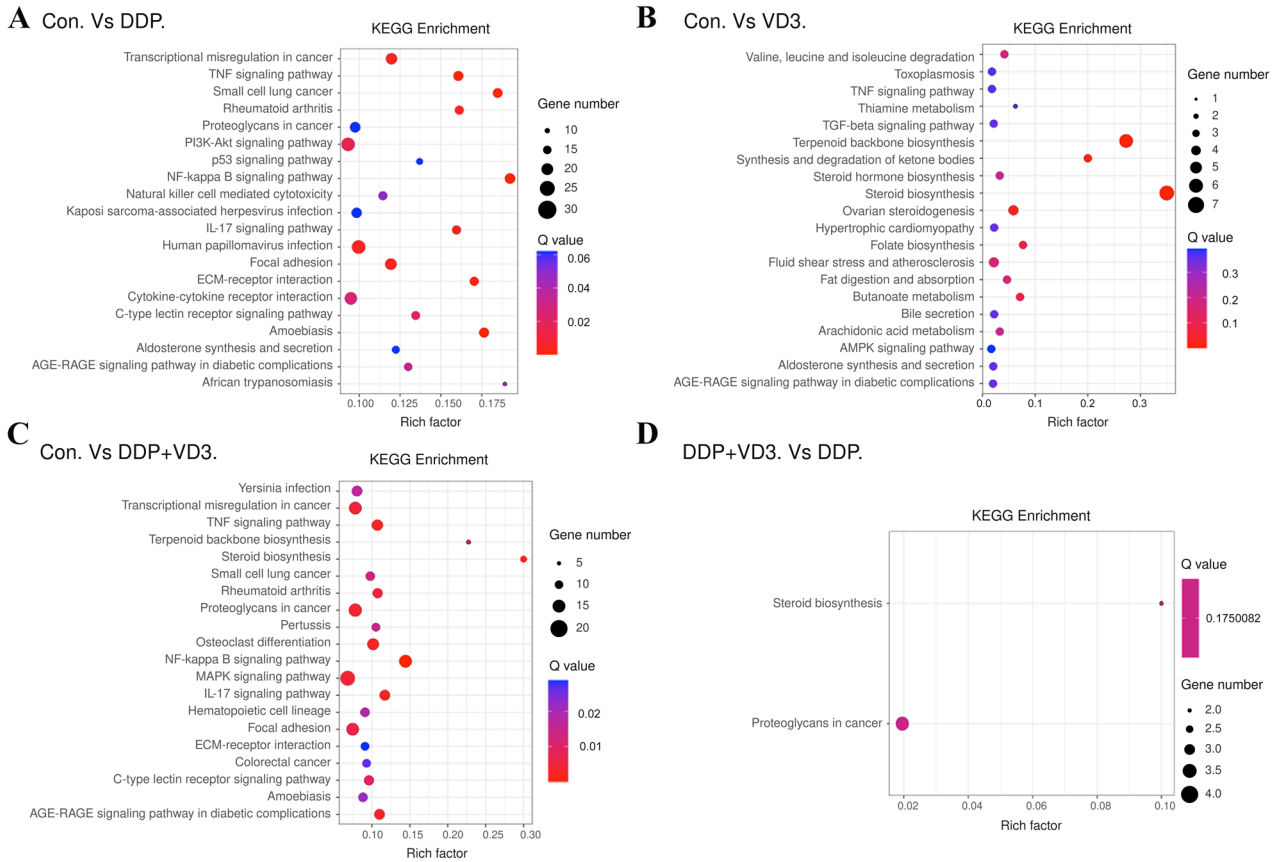

Figure 6. KEGG pathway enrichment analysis of DEGs. KEGG pathway enrichment analysis was performed using DEGs from the indicated comparison groups: Control vs. DDP (A), Control vs. VD_3 (B), Control vs. DDP plus VD_3 (C), and DDP vs. DDP plus VD_3 (D).

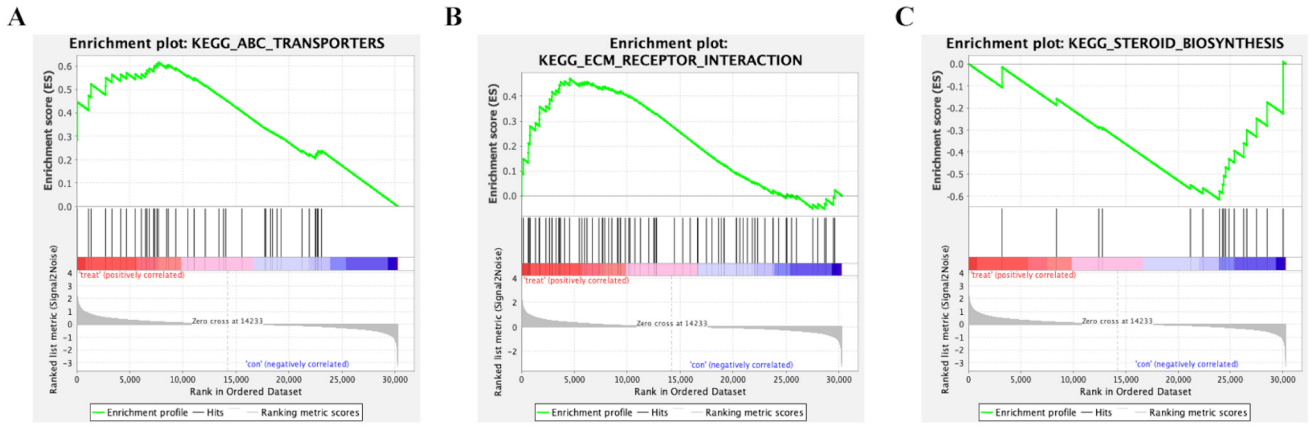

Figure 7. GSEA of pathway-level changes associated with VD_3 treatment in DDP-treated HGC-27 cells. GSEA was performed using RNA-seq data from HGC-27 cells treated with DDP plus VD_3 compared with cells treated with DDP alone. Representative enriched pathways include ABC transporter-related pathways (A), ECM-receptor interaction (B), and steroid biosynthesis (C).

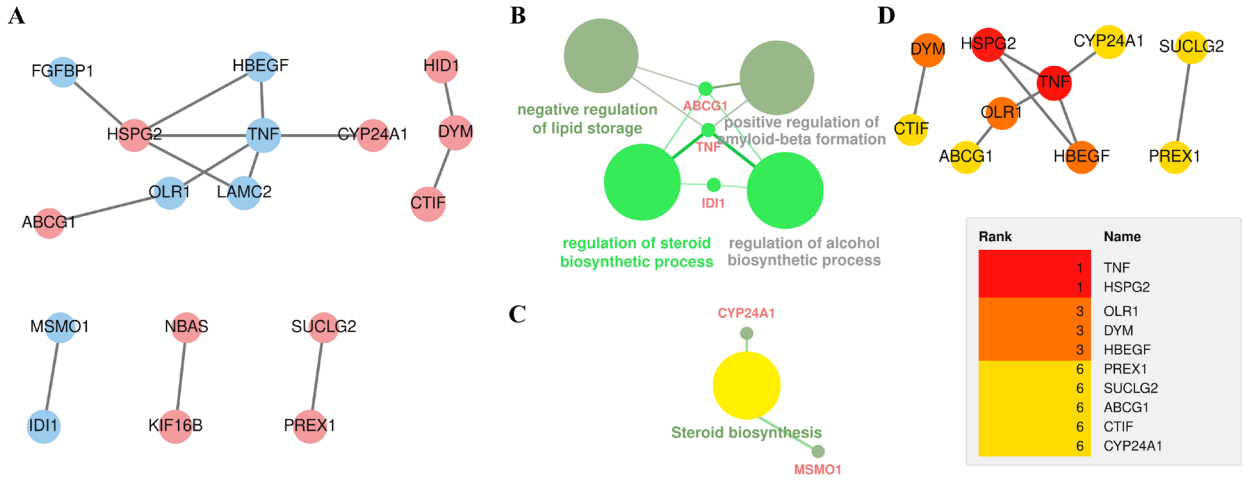

Figure 8. Protein-protein interaction network analysis of candidate genes associated with VD_3-mediated modulation of DDP response. A) PPI network constructed using DEGs identified in the DDP plus VD_3 versus DDP comparison. B) GO functional annotation analysis of genes included in the PPI network. C) KEGG pathway annotation analysis of genes included in the PPI network. D) Hub gene ranking based on network topology analysis using the cytoHubba plugin in Cytoscape. Candidate hub genes were identified according to their network scores.

porter activity, ECM signaling, and steroid metabolism in DDP-treated gastric cancer cells.

Protein interaction network analysis identifies candidate pathways and hub genes associated with VD_3 treatment. To further characterize the molecular networks associated with VD_3 treatment, a PPI network was constructed using the DEGs identified between the DDP plus VD_3 group and the DDP-alone group. Analysis using the STRING database generated a network comprising 17 nodes and 13 edges, including 10 upregulated and 7 downregulated genes (Figure 8A). The genes within this network were subsequently analyzed using the ClueGO plugin for GO-BP and KEGG enrichment analyses. GO-BP analysis indicated enrichment of biological processes related to the negative regulation of lipid storage and the regulation of steroid biosynthetic processes (Figure 8B). Consistent with these findings, KEGG analysis identified steroid biosynthesis as the principal enriched pathway associated with VD_3 treatment (Figure 8C). To identify key regulatory genes within the network, hub gene analysis was performed using the CytoHubba plugin. *TNF* and *HSPG2* were identified as the highest-ranking hub genes and may represent important components of the transcriptional network associated with VD_3 treatment in DDP-exposed gastric cancer cells (Figure 8D).

Protein-protein interaction network analysis of genes no longer differentially expressed after VD_3 co-treatment. To further investigate the transcriptional changes attenuated by VD_3, we performed PPI network analysis on genes that

were differentially expressed following DDP treatment but were no longer significantly altered after co-treatment with VD_3. The resulting PPI network comprised 427 nodes and 875 edges (Supplementary Figure S5A). These genes were subsequently analyzed using the MCODE plugin to identify highly interconnected subnetworks, yielding two core subnetworks with MCODE scores greater than 6 (Supplementary Figures S5B, S5C).

Functional annotation of genes within these subnetworks was performed using the ClueGO plugin. GO-BP analysis revealed significant enrichment of biological processes related to collagen-activated tyrosine kinase receptor signaling, whereas KEGG analysis identified ECM-receptor interaction as a major enriched pathway (Supplementary Figures S5D, S5E). These results suggest that genes whose DDP-induced expression changes were attenuated by VD_3 are primarily associated with tyrosine kinase receptor signaling and ECM-related pathways. These findings indicate that VD_3 may modulate transcriptional programs involved in these pathways in DDP-treated gastric cancer cells.

Discussion

DDP exerts its antitumor activity through multiple mechanisms, most notably by forming DNA adducts through interactions with purine bases, thereby inducing DNA damage, activating intracellular signaling pathways, and ultimately triggering apoptosis. However, treatment-related toxicity and acquired drug resistance remain major obstacles that limit its clinical efficacy. Therefore, elucidating the molecular mechanisms underlying DDP resistance is essential for improving therapeutic outcomes. Reduced intracellular drug accumulation, detoxification by glutathione and metallothioneins, and enhanced DNA damage repair have all been implicated in the development of DDP resistance [36]. In the present study, VD_3 attenuated DDP-induced cytotoxicity in gastric cancer cell lines under *in vitro* conditions, suggesting that VD_3 exposure may reduce DDP sensitivity in certain cellular contexts. Consistent with this observation, apoptosis assays demonstrated that the reduced cytotoxic response was associated, at least in part, with decreased DDP-induced apoptosis. DDP is known to induce DNA double-strand breaks (DSBs), which initiate a cascade of signaling events that ultimately lead to apoptotic cell death [37, 38]. Previous studies have reported a strong positive correlation between DSB formation and γH2AX accumulation, supporting the use of γH2AX as a marker of DNA damage response activation [39]. In agreement with these findings, our western blot analyses showed that DDP treatment markedly increased γH2AX levels in gastric cancer cells, indicating activation of DNA damage-associated signaling pathways. Because DDP-induced DNA lesions activate the cellular DNA damage response, γH2AX is widely used as an indicator of this process, particularly following DSB formation. Nevertheless, γH2AX should be interpreted cautiously because it reflects activation of DNA damage-associated signaling rather than DNA repair capacity itself [40]. In our study, co-treatment with VD_3 reduced DDP-induced γH2AX accumulation, suggesting attenuation of DNA damage-associated signaling. However, this finding should not be interpreted as evidence of enhanced DNA repair. γH2AX levels can be influenced by multiple factors, including the extent of DNA damage, ROS-associated stress, apoptotic cell fraction, cell-cycle distribution, and upstream DNA damage response signaling. Therefore, although our results indicate that VD_3 attenuates DDP-induced γH2AX activation, additional functional studies are required to determine whether VD_3 directly affects DNA repair processes or influences other mechanisms involved in the cellular response to DDP.

ROS are continuously generated as byproducts of mitochondrial oxidative metabolism under physiological conditions. Maintenance of ROS homeostasis is essential for normal cellular survival and signal transduction [41]. However, excessive ROS accumulation can disrupt mitochondrial function, activate mitochondrial apoptotic pathways, and induce oxidative damage to cellular macromolecules, including DNA [42–45]. Previous studies have shown that DDP promotes intracellular ROS generation, which may further exacerbate DNA damage and contribute to apoptosis through both oxidative stress-dependent and mitochondrial pathways [46]. In the present study, we evaluated the effects of DDP and VD_3 on oxidative stress in gastric cancer cells. Consistent with previous reports, DDP treatment markedly increased intracellular ROS levels. In contrast, co-treatment with VD_3 significantly attenuated DDP-induced ROS accumulation. These findings suggest that VD_3 mitigates the oxidative stress response triggered by DDP. Given the established links between ROS accumulation, DNA damage signaling, and apoptosis, the reduction in ROS levels may partially contribute to the decreased γH2AX accumulation, reduced apoptosis, and attenuated cytotoxicity observed following VD_3 co-treatment. However, the precise mechanisms underlying these effects remain to be elucidated.

Our experimental findings demonstrated that VD_3 attenuated the cytotoxic effects of DDP in gastric cancer cells under *in vitro* conditions. To gain further insight into the molecular basis of this phenomenon, we performed transcriptomic analyses of cells treated with DDP, VD_3, DDP plus VD_3, or vehicle control. DDP treatment induced extensive transcriptional alterations, affecting genes involved in several pathways, including NF-κB signaling, ECM-receptor interaction, and TNF signaling. In contrast, VD_3 treatment alone primarily affected genes associated with steroid metabolism. Given that VD_3 is a steroid-derived molecule, modulation of steroid metabolic pathways is consistent with its known biological activity. Notably, co-treatment with VD_3 markedly reduced the number of DDP-responsive DEGs, suggesting that VD_3 modifies the transcriptional response to DDP. Functional enrichment analyses indicated that many of the genes whose DDP-induced expression changes were attenu-

ated by VD_3 were associated with DNA damage response-related processes and ECM-receptor interaction pathways. These observations suggest that VD_3 may influence transcriptional programs affected by DDP, particularly those related to DNA damage-associated signaling and extracellular matrix regulation; however, direct functional validation is required to establish causal relationships. To further support the transcriptomic findings, representative genes identified by RNA-seq, including *CYP24A1*, *HMGCR*, *GDF15*, *CDKN1A*, and *SPIDR*, were evaluated by qRT-PCR. The expression patterns obtained by qRT-PCR were generally consistent with the RNA-seq results, supporting the reliability of the transcriptomic analysis.

Direct comparison between the DDP plus VD_3 group and the DDP-alone group further revealed transcriptomic changes associated with steroid metabolic processes, ECM-receptor interaction, and ABC transporter-related pathways. GSEA additionally identified enrichment of gene sets related to ABC transporters and ECM-receptor interaction, together with negative enrichment of steroid biosynthesis-related genes following VD_3 co-treatment. Because ABC transporters are well-recognized mediators of drug efflux and chemoresistance, these findings raise the possibility that altered transporter-related transcriptional programs may contribute to the reduced DDP sensitivity observed in VD_3-treated cells. However, the current data are based primarily on transcriptomic analyses and do not establish functional changes in transporter activity. Finally, PPI network analysis identified *TNF* and *HSPG2* as candidate hub genes within the VD_3-associated transcriptional network. Future studies are required to determine whether these genes, or other candidate regulators identified in this study, functionally contribute to the modulation of DDP responses by VD_3.

Several limitations of this study should be acknowledged. First, the experiments were conducted primarily in established gastric cancer cell lines and evaluated short-term drug responses under *in vitro* conditions. Consequently, the findings require validation in animal models, patient-derived systems, and clinical samples. Moreover, *in vitro* models cannot fully recapitulate the pharmacokinetics of DDP, systemic vitamin D metabolism, the tumor microenvironment, immune regulation, or patient-specific vitamin D status. Second, the compound examined in this study was VD_3/cholecalciferol, a precursor form of vitamin D, rather than the hormonally active metabolite 1,25-dihydroxyvitamin D_3. Intracellular conversion of cholecalciferol to 25-hydroxyvitamin D_3, 1,25-dihydroxyvitamin D_3, or non-classical vitamin D-derived metabolites was not directly evaluated. Previous studies have shown that CYP11A1-derived vitamin D and lumisterol metabolites participate in the regulation of oxidative stress, DNA damage responses, inflammation, and cell proliferation, and that both classical and CYP11A1-derived vitamin D hydroxyderivatives exhibit anticancer activity in basal and squamous cell carcinoma models [15, 16]. Therefore, whether these metabolites contribute to the observed changes in ROS accumulation, γH2AX activation, apoptosis, and DDP sensitivity remains to be determined. Third, DNA repair activity was not directly assessed. Although γH2AX was used as a marker of DDP-induced DNA damage response activation, reduced γH2AX accumulation cannot distinguish between decreased DNA damage generation, altered repair kinetics, reduced apoptosis, changes in cell-cycle distribution, or modulation of upstream DNA damage response signaling pathways. Accordingly, the present data do not establish a direct effect of VD_3 on DNA repair capacity. Finally, although selected RNA-seq findings were validated by qRT-PCR, the transcriptomic analyses remain largely correlative. Additional mechanistic studies are required to identify the direct molecular mediators responsible for the VD_3-associated modulation of DDP responses. Therefore, the results of this study should be interpreted with caution and should not be directly extrapolated to clinical recommendations regarding vitamin D supplementation during DDP-based chemotherapy.

In summary, the present study demonstrates that VD_3 attenuates DDP-induced cytotoxicity, apoptosis, ROS accumulation, and γH2AX activation in gastric cancer cells under *in vitro* conditions. Transcriptomic analyses further suggest that VD_3 modulates gene expression programs associated with steroid metabolism, ECM-related pathways, ABC transporter-associated pathways, and DNA damage response-related processes. Collectively, these findings provide preliminary evidence that VD_3 exposure can influence cellular responses to DDP in gastric cancer cells. However, the specific vitamin D-derived metabolites involved, the underlying molecular mechanisms, and the clinical relevance of these observations remain to be elucidated through further mechanistic, preclinical, and clinical studies.

Supplementary information is available in the online version of the paper.

Acknowledgments: This study was supported by the Zhejiang Province Basic Public Welfare Research Project (LGF22H030010 to KC).

References

[1] BRAY F, FERLAY J, SOERJOMATARAM I, SIEGEL RL, TORRE LA et al. Global cancer statistics 2018: GLOBOCAN estimates of incidence and mortality worldwide for 36 cancers in 185 countries. CA Cancer J Clin 2018; 68: 394–424. https://doi.org/10.3322/caac.21492

[2] CHEN W, ZHENG R, BAADE PD, ZHANG S, ZENG H et al. Cancer statistics in China, 2015. CA Cancer J Clin 2016; 66: 115–132. https://doi.org/10.3322/caac.21338

[3] LIU H, WU W, LIU Y, ZHANG C, ZHOU Z. Predictive value of cystic fibrosis transmembrane conductance regulator (CFTR) in the diagnosis of gastric cancer. Clin Invest Med. 2014; 37: E226–232. https://doi.org/10.25011/cim.v37i4.21728

[4] ZHAO TT, XU H, XU HM, WANG ZN, XU YY et al. The efficacy and safety of targeted therapy with or without chemotherapy in advanced gastric cancer treatment: a network meta-analysis of well-designed randomized controlled trials. Gastric Cancer 2018; 21: 361–371. https://doi.org/10.1007/s10120-018-0813-2

[5] MARIN JJ, AL-ABDULLA R, LOZANO E, BRIZ O, BUJANDA L et al. Mechanisms of Resistance to Chemotherapy in Gastric Cancer. Anticancer Agents Med Chem 2016; 16: 318–334. https://doi.org/10.2174/1871520615666150803125121

[6] JULIACHS M, MUNOZ C, MOUTINHO CA, VIDAL A, CONDOM E et al. The PDGFRbeta-AKT pathway contributes to CDDP-acquired resistance in testicular germ cell tumors. Clin Cancer Res 2014; 20: 658–667. https://doi.org/10.1158/1078-0432.CCR-13-1131

[7] BENEDETTI G, FREDRIKSSON L, HERPERS B, MEERMAN J, VAN DE WATER B et al. TNF-alpha-mediated NF-kappaB survival signaling impairment by cisplatin enhances JNK activation allowing synergistic apoptosis of renal proximal tubular cells. Biochem Pharmacol 2013; 85: 274–286. https://doi.org/10.1016/j.bcp.2012.10.012

[8] LIN CC, YEH HH, HUANG WL, YAN JJ, LAI WW et al. Metformin enhances cisplatin cytotoxicity by suppressing signal transducer and activator of transcription-3 activity independently of the liver kinase B1-AMP-activated protein kinase pathway. Am J Respir Cell Mol Biol 2013; 49: 241–250. https://doi.org/10.1165/rcmb.2012-0244OC

[9] GUEGAN JP, EZAN F, THERET N, LANGOUET S, BAFFET G. MAPK signaling in cisplatin-induced death: predominant role of ERK1 over ERK2 in human hepatocellular carcinoma cells. Carcinogenesis 2013; 34: 38–47. https://doi.org/10.1093/carcin/bgs317

[10] LI Z, SHU X, LIU X, LI Q, HU Y et al. Cellular and Molecular Mechanisms of Chemoresistance for Gastric Cancer. Int J Gen Med 2024; 17: 3779–3788. https://doi.org/10.2147/IJGM.S473749

[11] OZCAN G. The hypoxia-inducible factor-1alpha in stemness and resistance to chemotherapy in gastric cancer: Future directions for therapeutic targeting. Front Cell Dev Biol 2023; 11: 1082057. https://doi.org/10.3389/fcell.2023.1082057

[12] SLOMINSKI AT, TUCKEY RC, SLOMINSKI RM, HOLICK MF, JETTEN AM. On the role of cholesterol, vitamin D, lumisterol, and tachysterol signaling in psoriasis. J Invest Dermatol 2026; 146: 887–889. https://doi.org/10.1016/j.jid.2026.01.005

[13] ADAMS JS, HEWISON M. Extrarenal expression of the 25-hydroxyvitamin D-1-hydroxylase. Arch Biochem Biophys 2012; 523: 95–102. https://doi.org/10.1016/j.abb.2012.02.016

[14] TOWNSEND K, BANWELL CM, GUY M, COLSTON KW, MANSI JL et al. Autocrine metabolism of vitamin D in normal and malignant breast tissue. Clin Cancer Res 2005; 11: 3579–3586. https://doi.org/10.1158/1078-0432.CCR-04-2359

[15] SLOMINSKI AT, KIM TK, JANJETOVIC Z, SLOMINSKI RM, LI W et al. Biological Effects of CYP11A1-Derived Vitamin D and Lumisterol Metabolites in the Skin. J Invest Dermatol 2024; 144: 2145–2161. https://doi.org/10.1016/j.jid.2024.04.022

[16] SLOMINSKI AT, BROZYNA AA, KIM TK, ELSAYED MM, JANJETOVIC Z et al. CYP11A1-derived vitamin D hydroxyderivatives as candidates for therapy of basal and squamous cell carcinomas. Int J Oncol 2022; 61: 96. https://doi.org/10.3892/ijo.2022.5386

[17] SLOMINSKI AT, SLOMINSKI RM, KAMAL M, HOLICK MF, TUCKEY RC et al. Is Vitamin D Signaling Regulated by and Does It Regulate Circadian Rhythms? FASEB J 2025; 39: e71321. https://doi.org/10.1096/fj.202503003R

[18] DAKSHINAMURTI K. Vitamins and their derivatives in the prevention and treatment of metabolic syndrome diseases (diabetes). Can J Physiol Pharmacol 2015; 93: 355–362. https://doi.org/10.1139/cjpp-2014-0479

[19] BRUSTAD N, STOKHOLM J, BONNELYKKE K, CHAWES BL. Vitamin D-FUT2 interaction and risk of lower respiratory tract infections in childhood. Allergy 2025; 80: 582–584. https://doi.org/10.1111/all.16266

[20] GIAMPAZOLIAS E, PEREIRA DA COSTA M, LAM KC, LIM KHJ, CARDOSO A et al. Vitamin D regulates microbiome-dependent cancer immunity. Science 2024; 384: 428–437. https://doi.org/10.1126/science.adh7954

[21] DE LA GUIA-GALIPIENSO F, MARTINEZ-FERRAN M, VALLECILLO N, LAVIE CJ, SANCHIS-GOMAR F et al. Vitamin D and cardiovascular health. Clin Nutr 2021; 40: 2946–2957. https://doi.org/10.1016/j.clnu.2020.12.025

[22] MANSON JE, COOK NR, LEE IM, CHRISTEN W, BASSUK SS et al. Vitamin D Supplements and Prevention of Cancer and Cardiovascular Disease. N Engl J Med 2019; 380: 33–44. https://doi.org/10.1056/NEJMoa1809944

[23] KUZNIA S, ZHU A, AKUTSU T, BURING JE, CAMARGO CA JR et al. Efficacy of vitamin D(3) supplementation on cancer mortality: Systematic review and individual patient data meta-analysis of randomised controlled trials. Ageing Res Rev 2023; 87: 101923. https://doi.org/10.1016/j.arr.2023.101923

[24] BERNHARDT SM, BORGES VF, SCHEDIN P. Vitamin D as a Potential Preventive Agent For Young Women's Breast Cancer. Cancer Prev Res (Phila) 2021; 14: 825–838. https://doi.org/10.1158/1940-6207.CAPR-21-0114

[25] SKRAJNOWSKA D, BOBROWSKA-KORCZAK B. Potential Molecular Mechanisms of the Anti-cancer Activity of Vitamin D. Anticancer Res 2019; 39: 3353–3363. https://doi.org/10.21873/anticanres.13478

[26] SUNIL KUMAR BV, SINGH S, VERMA R. Anticancer potential of dietary vitamin D and ascorbic acid: A review. Crit Rev Food Sci Nutr 2017; 57: 2623–2635. https://doi.org/10.1080/10408398.2015.1064086

[27] TOUVIER M, CHAN DS, LAU R, AUNE D, VIEIRA R et al. Meta-analyses of vitamin D intake, 25-hydroxyvitamin D status, vitamin D receptor polymorphisms, and colorectal cancer risk. Cancer Epidemiol Biomarkers Prev 2011; 20: 1003–1016. https://doi.org/10.1158/1055-9965.EPI-10-1141

[28] SLATTERY ML, WOLFF RK, HERRICK JS, CAAN BJ, SAMOWITZ W. Calcium, vitamin D, VDR genotypes, and epigenetic and genetic changes in rectal tumors. Nutr Cancer 2010; 62: 436–442. https://doi.org/10.1080/01635580903441204

[29] CHO E, SMITH-WARNER SA, SPIEGELMAN D, BEESON WL, VAN DEN BRANDT PA et al. Dairy foods, calcium, and colorectal cancer: a pooled analysis of 10 cohort studies. J Natl Cancer Inst 2004; 96: 1015–1022. https://doi.org/10.1093/jnci/djh185

[30] KOTLARZ A, PRZYBYSZEWSKA M, SWOBODA P, MILOSZEWSKA J, GRYGOROWICZ MA et al. Differential interference of vitamin D analogs PRI-1906, PRI-2191, and PRI-2205 with the renewal of human colon cancer cells refractory to treatment with 5-fluorouracil. Tumour Biol 2016; 37: 4699–4709. https://doi.org/10.1007/s13277-015-4311-4

[31] SANTOS JM, HUSSAIN F. VD(3) mitigates breast cancer aggressiveness by targeting V-H(+)-ATPase. J Nutr Biochem 2019; 70: 185–193. https://doi.org/10.1016/j.jnutbio.2019.05.005

[32] LIU Y, WANG X, SUN X, LU S, LIU S. Vitamin intake and pancreatic cancer risk reduction: A meta-analysis of observational studies. Medicine (Baltimore) 2018; 97: e0114. https://doi.org/10.1097/MD.0000000000010114

[33] GILZAD-KOHAN H, SANI S, BOROUJERDI M. Calcitriol Reverses Induced Expression of Efflux Proteins and Potentiates Cytotoxic Activity of Gemcitabine in Capan-2 Pancreatic Cancer Cells. J Pharm Pharm Sci 2017; 20: 295–304. https://doi.org/10.18433/J37W7R

[34] BOSTICK RM. Effects of supplemental vitamin D and calcium on normal colon tissue and circulating biomarkers of risk for colorectal neoplasms. J Steroid Biochem Mol Biol 2015; 148: 86–95. https://doi.org/10.1016/j.jsbmb.2015.01.010

[35] BOCHEN F, BALENSIEFER B, KORNER S, BITTENBRING JT, NEUMANN F et al. Vitamin D deficiency in head and neck cancer patients – prevalence, prognostic value and impact on immune function. Oncoimmunology 2018; 7: e1476817. https://doi.org/10.1080/2162402X.2018.1476817

[36] GHOSH S. Cisplatin: The first metal based anticancer drug. Bioorg Chem 2019; 88: 102925. https://doi.org/10.1016/j.bioorg.2019.102925

[37] SANCHO-MARTINEZ SM, PRIETO-GARCIA L, PRIETO M, LOPEZ-NOVOA JM, LOPEZ-HERNANDEZ FJ. Subcellular targets of cisplatin cytotoxicity: an integrated view. Pharmacol Ther 2012; 136: 35–55. https://doi.org/10.1016/j.pharmthera.2012.07.003

[38] BASU A, KRISHNAMURTHY S. Cellular responses to Cisplatin-induced DNA damage. J Nucleic Acids 2010; 2010: 201367. https://doi.org/10.4061/2010/201367

[39] ROTHKAMM K, LOBRICH M. Evidence for a lack of DNA double-strand break repair in human cells exposed to very low x-ray doses. Proc Natl Acad Sci U S A 2003; 100: 5057–5062. https://doi.org/10.1073/pnas.0830918100

[40] VALENTE D, GENTILESCHI MP, GUERRISI A, BRUZZANITI V, MORRONE A et al. Factors to Consider for the Correct Use of gammaH2AX in the Evaluation of DNA Double-Strand Breaks Damage Caused by Ionizing Radiation. Cancers (Basel) 2022; 14: 6204. https://doi.org/10.3390/cancers14246204

[41] EBRAHIMI SO, REIISI S, SHAREEF S. miRNAs, oxidative stress, and cancer: A comprehensive and updated review. J Cell Physiol 2020; 235: 8812–8825. https://doi.org/10.1002/jcp.29724

[42] MA L, WANG H, WANG C, SU J, XIE Q et al. Failure of Elevating Calcium Induces Oxidative Stress Tolerance and Imparts Cisplatin Resistance in Ovarian Cancer Cells. Aging Dis 2016; 7: 254–266. https://doi.org/10.14336/AD.2016.0118

[43] LIN L, ZHENG J, ZHU W, JIA N. Nephroprotective effect of gelsemine against cisplatin-induced toxicity is mediated via attenuation of oxidative stress. Cell Biochem Biophys 2015; 71: 535–541. https://doi.org/10.1007/s12013-014-0231-y

[44] IKNER A, SHIOZAKI K. Yeast signaling pathways in the oxidative stress response. Mutat Res 2005; 569: 13–27. https://doi.org/10.1016/j.mrfmmm.2004.09.006

[45] BARZILAI A, ROTMAN G, SHILOH Y. ATM deficiency and oxidative stress: a new dimension of defective response to DNA damage. DNA Repair (Amst) 2002; 1: 3–25. https://doi.org/10.1016/s1568-7864(01)00007-6

[46] GALLUZZI L, SENOVILLA L, VITALE I, MICHELS J, MARTINS I et al. Molecular mechanisms of cisplatin resistance. Oncogene 2012; 31: 1869–1883. https://doi.org/10.1038/onc.2011.384

https://doi.org/10.4149/neo_2026_260310N61

Transcriptomic analysis of vitamin D3 (cholecalciferol)-mediated attenuation of cisplatin sensitivity in gastric cancer cells *in vitro*

Ke CHEN*, Yu PAN

Supplementary Information

Supplementary Table S1. Primer sequences used for qRT-PCR.

Gene	Primer	Sequence (5'–3')
CYP24A1	Forward	GACCTGATGAGCCTGACGGC
	Reverse	GAGGGGCTTTGGTATCCGCC
HMGCR	Forward	ACACTTTGGGGAGGCCAACG
	Reverse	ACATCCACCTCCCGGGTTCA
GDF15	Forward	TTGTACCAGCCTGAGGGGCT
	Reverse	ACTGCCCAGGCTGCAATGTT
CDKN1A	Forward	GCGGGTGCGGTGATGGATAA
	Reverse	GTGGGCGGATTAGGGCTTCC
SPIDR	Forward	GCCGAGACAGGTGGATCACG
	Reverse	GCACCATCACGCCCGGATAA
GAPDH	Forward	GCGGGGCTCTCCAGAACATC
	Reverse	TCCACCACTGACACGTTGGC

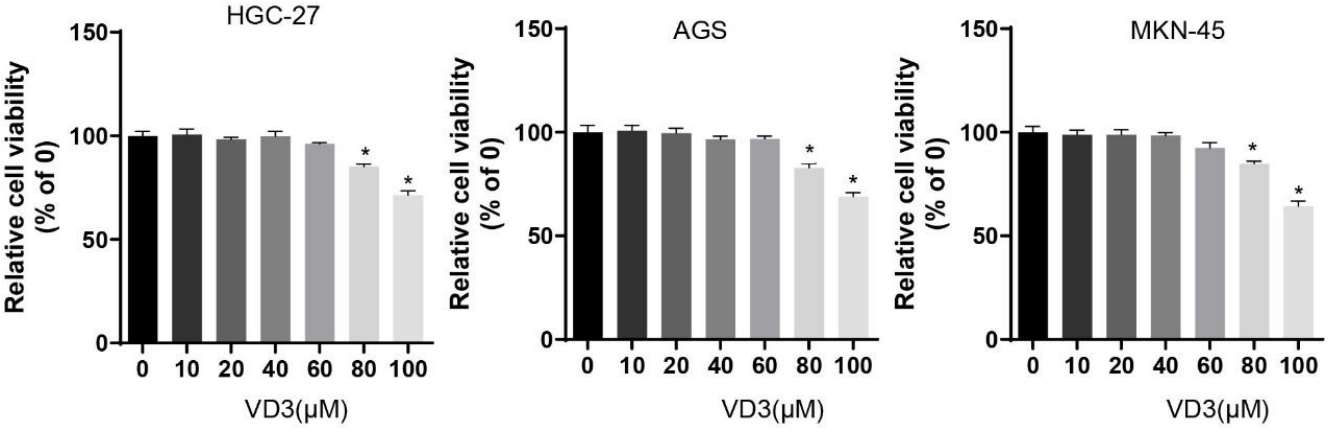

Supplementary Figure S1. Effects of VD_3 on gastric cancer cell viability. HGC-27, AGS, and MKN-45 cells were treated with increasing concentrations of VD_3 (0, 10, 20, 40, 60, 80, and 100 μM) for 24 h, and cell viability was assessed using the CCK-8 assay. Cell viability was normalized to the untreated control group (0 μM). Data are presented as the mean±SD of three independent experiments. Statistical significance was determined by one-way ANOVA. *p<0.05 vs. the untreated control group

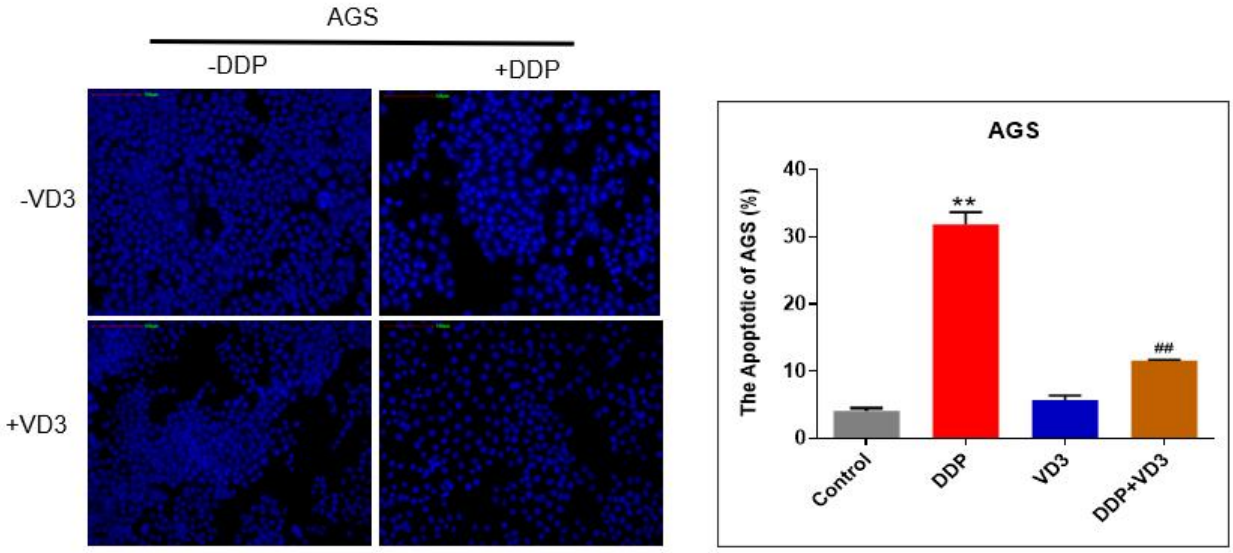

Supplementary Figure S2. Hoechst staining analysis of apoptosis in AGS cells following treatment with DDP and VD_3. AGS cells were treated with vehicle control, VD_3, DDP, or DDP plus VD_3 for 24 h. Apoptosis was assessed by Hoechst staining. Representative fluorescence images and corresponding quantitative analysis are shown. Data are presented as the mean±SD of three independent experiments. Statistical significance was determined by one-way ANOVA. $^{**}p<0.01$ vs. the control group; $^{\#\#}p<0.01$ vs. the DDP-treated group

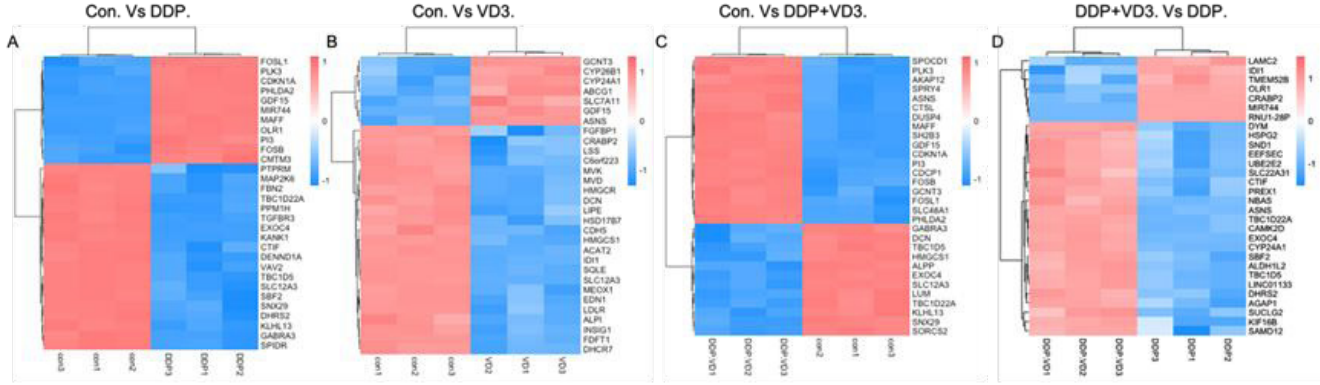

Supplementary Figure S3. Differential gene expression patterns associated with VD_3 and DDP treatment in HGC-27 cells. Heatmaps showing the top 30 differentially expressed genes in the Control vs. DDP (A), Control vs. VD_3 (B), Control vs. DDP plus VD_3 (C), and DDP vs. DDP plus VD_3 (D) comparisons.

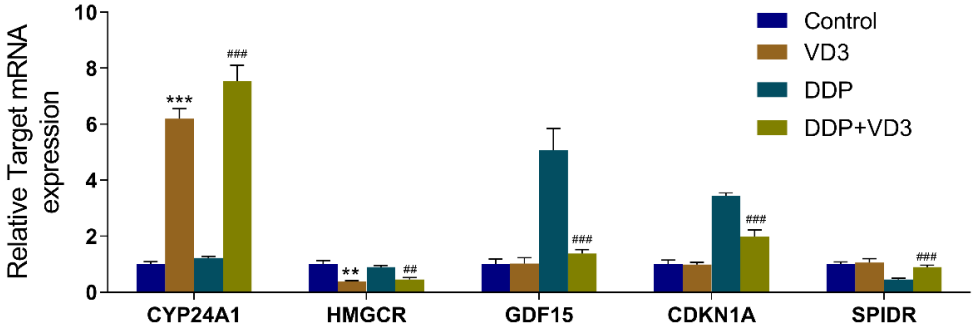

Supplementary Figure S4. qRT-PCR validation of representative RNA-seq genes. Relative mRNA expression levels of CYP24A1, HMGCR, GDF15, CDKN1A, and SPIDR were measured in HGC-27 cells following treatment with vehicle control, VD_3, DDP, or DDP plus VD_3 for 24 h. GAPDH was used as the internal control. Relative gene expression was calculated using the $2^{-\Delta\Delta Ct}$ method and normalized to the control group. Data are presented as the mean±SD of three independent experiments. Statistical significance was determined by one-way ANOVA. $^{***}p<0.001$ vs. the control group; $^{\#\#\#}p<0.001$ vs. the DDP-treated group

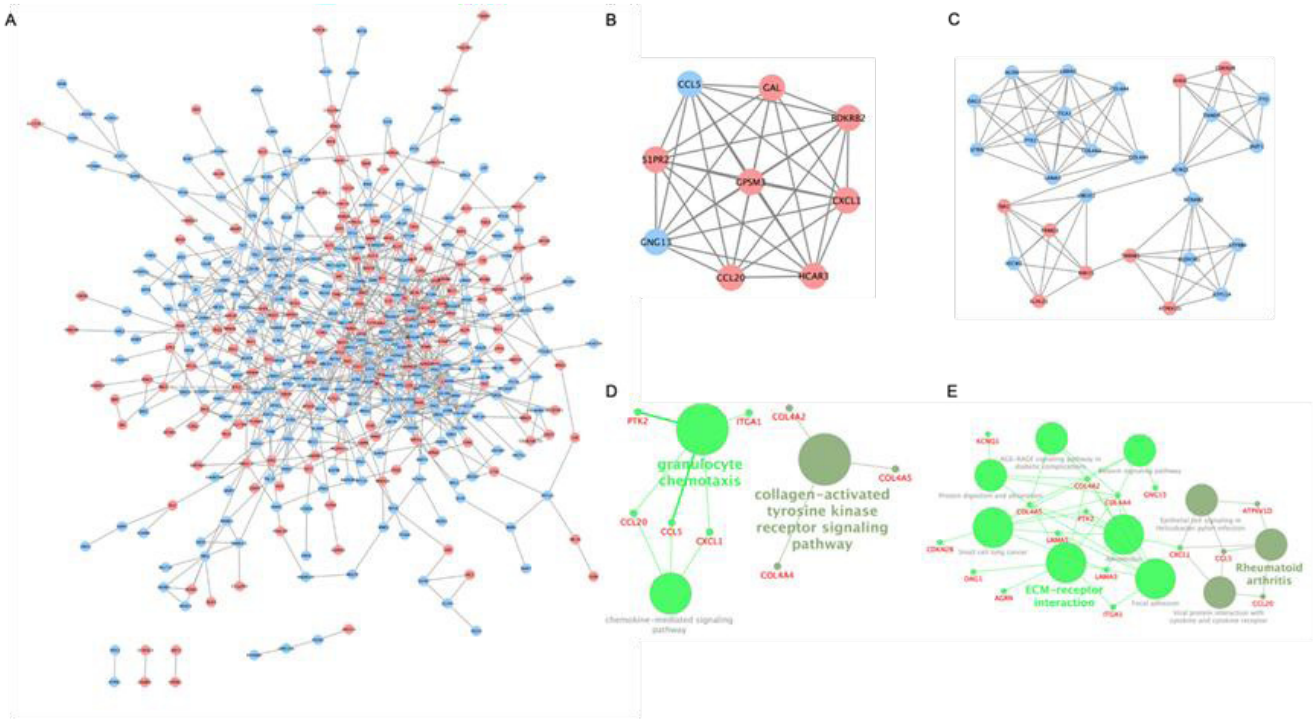

Supplementary Figure S5. Protein–protein interaction network analysis of genes whose DDP-induced expression changes were attenuated by VD_3. A) PPI network constructed using genes that were differentially expressed following DDP treatment but were no longer significantly differentially expressed after co-treatment with VD_3. B–C) Subnetwork analysis of PPI network genes using the MCODE algorithm (selection threshold: MCODE score >6). D, E) GO and KEGG enrichment analyses of genes within the selected subnetworks.